minerals

Article

Magma Sources and Tectonic Settings of Concealed Intrusive Rocks in the Jinchang Ore District, Yanbian–Dongning Region, Northeast China: Zircon U–Pb Geochronological, Geochemical, and Hf Isotopic Evidence

Zhigao Wang [1,*], Wenyan Cai [2], Shunda Li [3] and Xuli Ma [4]

1 College of Earth Sciences, Jilin University, Changchun 130061, China
2 School of Resources and Environmental Engineering, Shandong University of Technology, Zibo 255000, China; caiwy@sdut.edu.cn
3 College of Geology and Mining Engineering, Xinjiang University, Urumqi 830047, China; shunda@xju.edu.cn
4 School of Resources, Environment and Architectural Engineering, Chifeng University, Chifeng 024000, China; msnow2022@163.com
* Correspondence: wangzg19@jlu.edu.cn

Abstract: The Jinchang deposit is a large Au deposit in the Yanbian–Dongning region, in Northeast China, and is the product of magmatic–hydrothermal activities related to Early Cretaceous concealed igneous intrusions. However, these Early Cretaceous ore-causative igneous intrusions and the ore-hosting rocks in the Jinchang ore district have rarely been studied, with their magma sources and tectonic settings being ambiguous. Here, we integrate new geochemical, zircon U–Pb and Hf isotopic data from the concealed ore-hosting monzogranite and the ore-causative granodiorite to constrain their magma sources and tectonic settings. Zircon U–Pb dating indicates that the two monzogranites from the drill holes J_IZKN01 and $J_{18}ZK0303$ have similar crystallization ages of 202.0 ± 1.6 and 200.9 ± 1.2 Ma, respectively, whereas the granodiorite from the drill hole $J_{XI\text{-}1}ZK1001$ was formed in the Early Cretaceous period (107.0 ± 3.0 Ma). They are all enriched in large-ion lithophile elements (e.g., Rb, Th, and K) and light rare-earth elements, depleted in high field strength elements (e.g., Nb, Ta, and Ti) and heavy rare-earth elements, and yield similar positive $\varepsilon Hf(t)$ values of +4.4 to +11.5, with their two-stage model ages ranging from 799 to 389 Ma. These results indicate that the concealed Early Jurassic ore-hosting monzogranite was derived from the partial melting of the Neoproterozoic–Paleozoic continental crust in a continental arc setting related to the Paleo-Pacific subduction. The ore-causative granodiorite originated from the partial melting of both the mantle wedge and the overlying continental crust, most likely caused by the dehydration and metasomatism of the subducted Paleo-Pacific slab involved in the rollback in the Early Cretaceous period.

Keywords: Jinchang ore district; geochemistry; zircon U–Pb dating; Hf isotope; Northeast China

check for updates

Citation: Wang, Z.; Cai, W.; Li, S.; Ma, X. Magma Sources and Tectonic Settings of Concealed Intrusive Rocks in the Jinchang Ore District, Yanbian–Dongning Region, Northeast China: Zircon U–Pb Geochronological, Geochemical, and Hf Isotopic Evidence. *Minerals* **2022**, *12*, 708. https://doi.org/10.3390/min12060708

Academic Editors: Zhuang Li, Zhiwei Wang and Sung Won Kim

Received: 22 April 2022
Accepted: 31 May 2022
Published: 1 June 2022

1. Introduction

The Yanbian–Dongning region, located at the eastern margin of Northeast China (Figure 1), mainly experienced the final closure of the Paleo-Asian Ocean in the late Permian–Middle Triassic [1–7] and the subduction of the Paleo-Pacific Plate in the Mesozoic–Cenozoic [6,8]. As a typical superposition area of the Paleo-Asian Ocean and Paleo-Pacific regimes, the Yanbian–Dongning region contains large-scale magmatic rocks and hosts a series of endogenous Early Cretaceous Au deposits of various types, including the large Jinchang porphyry Au deposit [9], the medium Naozhi intrusion-related Au deposit, and the small Jiusangou epithermal Au deposit [10]. The majority of the Au deposits are genetically related to the emplacement activities of the Early Cretaceous magmatic rocks, caused by the Paleo-Pacific subduction [9–11].

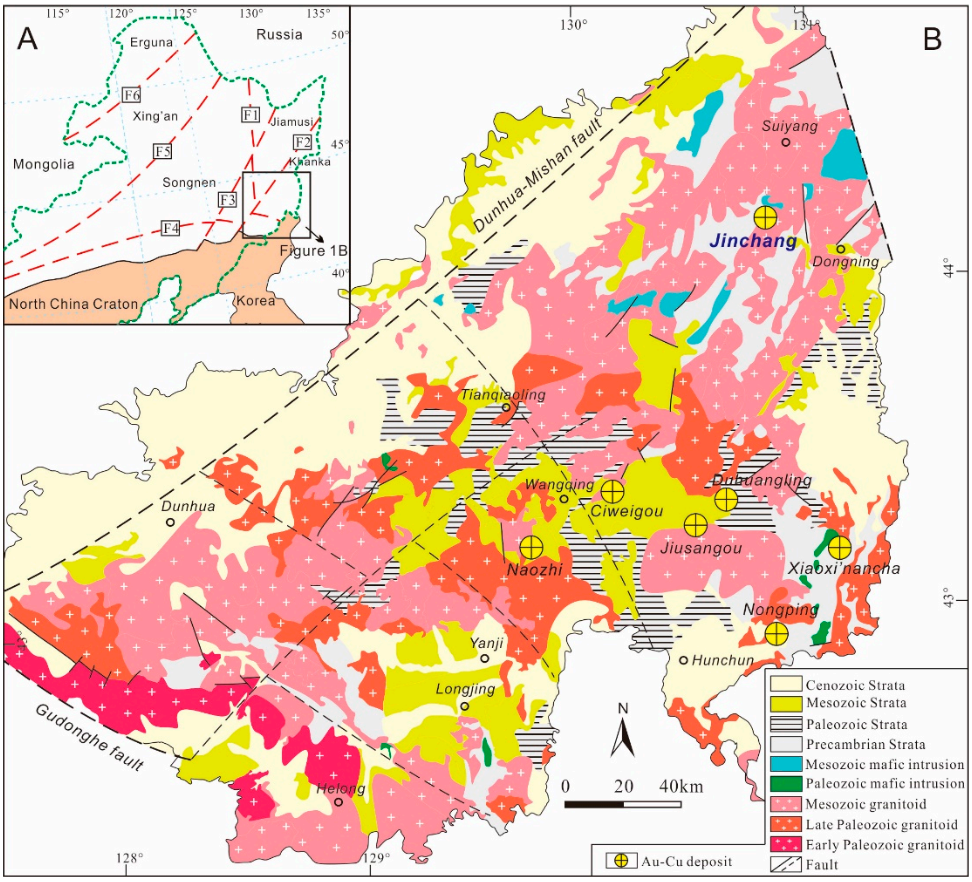

Figure 1. (**A**) Tectonic subdivisions of NE China (modified from Wu et al. [6]). Abbreviations: F1, Mudanjiang Fault; F2, Dunhua–Mishan Fault; F3, Yitong–Yilan Fault; F4, Xilamulun–Changchun Fault; F5, Hegenshan–Heihe Fault; F6, Tayuan–Xiguitu Fault. (**B**) Geologic map of the Yanbian–Dongning region, showing a range of representative gold deposits (modified from Wang [12]).

The Jinchang deposit is a large-sized representative Au deposit in the Yanbian–Dongning region and is characterized by three mineralization styles: the disseminated Au in granites, Au-bearing breccia pipes, and fault-controlled auriferous veins [9,12,13]. It was discovered in 1958 and contains a total of 80.947 tons of Au reserves [12]. As a crucial Au producer in Northeast China, the Jinchang deposit attracted considerable attention, with extensive studies being undertaken with the goal of documenting the ore fluid characteristics, mineralization ages, and ore genesis of this deposit [9,12–14]. Fluid inclusion and H–O–S isotope studies indicated that the ore-forming fluids of the Au mineralization belong to a high-temperature, high-salinity immiscible system and were derived from magmatic fluids; the sulfur in the sulfide detected in the Au ores originated from magmas [9,12]. The formation age of the Jinchang Au deposit was constrained to the Early Cretaceous (ca. 113–100 Ma) by sulfide Re–Os and quartz $^{40}Ar/^{39}Ar$ dating [9,13,14]. These results indicated that the Au mineralization was the product of magmatic–hydrothermal activities related to the Early Cretaceous igneous intrusions, although the widespread Early Jurassic granitoids acted as wall-rocks to host the three styles of Au mineralization in the Jinchang ore district. However, the Early Cretaceous igneous intrusions, associated with the Au mineralization, have received less attention, apart from several inessential porphyritic diorite dykes [15], with the available information being relatively scarce, probably because almost none of these intrusions are exposed at the surface. Cai et al. [9] reported that the concealed Early Cretaceous granodiorite was spatially, temporally, and genetically related to the Au mineralization. Nevertheless, the magma source of the granodiorite was unknown owing to a lack of detailed petrographic and necessary isotopic data. In addition, negligible information is available about the igneous rocks beneath both the largest J1

Au-bearing breccia pipe and the No. 18 disseminated Au orebodies, with the crystallization ages, magma sources, and tectonic settings of these concealed rocks being unclear.

In this study, we present new geochemical, zircon U–Pb, and Hf isotopic data for the concealed igneous rocks obtained from the Jinchang ore district. These results, combined with the age, geochemical, and isotopic data of both the Au ores and igneous rocks reported previously, provide clear constraints on the magma sources and tectonic settings of the ore-hosting and ore-causative rocks for the Au mineralization in the Jinchang ore district.

2. Geological Background

The Yanbian–Dongning region is located in the southeastern margin of Northeast China and separates the Khanka Massif from the North China Craton (Figure 1). This region is composed mainly of three geological units, i.e., the Taipingling continental margin zone, the Kaishantun accretionary complex zone, and the Seluohe thrusting accretionary zone [16–18]. Generally, the formation of accretionary zones is considered to be related to the Paleozoic subduction of the Paleo-Asian oceanic plate, the final closure of the intervening Paleo-Asian Ocean at ca. 250 Ma, and the subsequent collision orogeny along the Changchun–Yanji zone during the Early–Middle Triassic [6,18–23]. In view of the complex tectonic evolution, the Yanbian–Dongning region contains inconsistent stratigraphic units formed before the Middle Triassic. The northeastern Dongning area is mainly composed of the oldest Neoproterozoic middle-high-grade metamorphic rocks, Paleozoic terrigenous clastic rocks, and Middle-Lower Triassic volcanic rocks [12]. In contrast, the stratigraphic units of the southwestern Yanbian area consist of Silurian metasediments of low-amphibolite, high-green-schist facies, Upper Carboniferous marine limestones, Permian volcano-clastic rocks, and Lower Triassic volcanic rocks. Since the Middle Triassic, the Yanbian–Dongning region has undergone similar geological processes, with the strata mainly containing Upper Jurassic medium- and high-K calc-alkalic andesitic rocks and Cretaceous calc-alkaline basaltic andesite units [10].

The Yanbian–Dongning region has widely distributed large-scale igneous rocks, which can be divided into four emplacement stages of the late Permian–Early Triassic (270–240 Ma), Late Triassic (230–210 Ma), Early–Middle Jurassic (205–160 Ma), and Early Cretaceous (130–100 Ma) according to their zircon U–Pb ages [12]. Extensive Late Triassic–Middle Jurassic granitoids constitute the principal part of the intrusive rocks in this region (Figure 1B). In contrast, the Early Cretaceous intrusive rocks mainly occurred as granitoid and diorite stocks and as dykes that intruded into the pre-existing magmatic rocks. A series of Au deposits, such as the Jinchang, Xiaoxi'nancha, Naozhi, Ciweigou, and Nongping Au deposits (Figure 1B) are thought to be related to the magmatic activities in the Early Cretaceous [9–11,13–16,24–28].

3. Deposit Geology and Sample Descriptions

3.1. Ore District Geology

The Jinchang Au deposit is located ~32 km northwest of the Dongning City in the Yanbian–Dongning region (Figure 2). The Triassic Luoquanzhan Formation, exposed in the northwestern and southeastern parts of the ore district (Figure 2), primarily consists volcanic rock series, including dacitic breccia crystal tuff, andesitic crystal tuff, and hornblende andesite [9,12,13]. Structures in the ore district are dominated by a set of NE–SW-trending compressive shear faults (F1–F5) formed first, a set of NW–SE-trending compressive shear faults (F6–F7), a set of E–W-trending tensile faults (F8–F13), and a set of N–S-trending compressive faults (F14–F17; Figure 2). In addition, a set of well-developed ring fractures are distributed in the eastern ore district, and hosts a series of Au-bearing sulfide-quartz veins (Figure 2). The exposed igneous rocks in the ore district can be placed in six categories according to their petrography and zircon U–Pb ages, composed of a Late Triassic medium-grained diorite (209.5 ± 1.4 Ma) [15], an Early Jurassic medium- to fine-grained biotite granodiorite, fine-grained syenogranite, medium-grained monzogranite (206–185 Ma) [25,29–31], and the Early Cretaceous porphyritic diorite and granite porphyry

(Figure 2) [9,12]. The Late Triassic diorite and the Early Jurassic granitoids occupy the majority of the ore district, whereas the Early Cretaceous porphyritic diorite and granite porphyry generally occur as small NE–SW-trending dykes that intrude the older intrusions (Figure 2). In addition, two concealed igneous rocks, monzonite and granodiorite near the J0 and J11 Au-bearing breccia pipes, are constrained to 115 ± 3 and 107 ± 2 Ma, respectively [9,12].

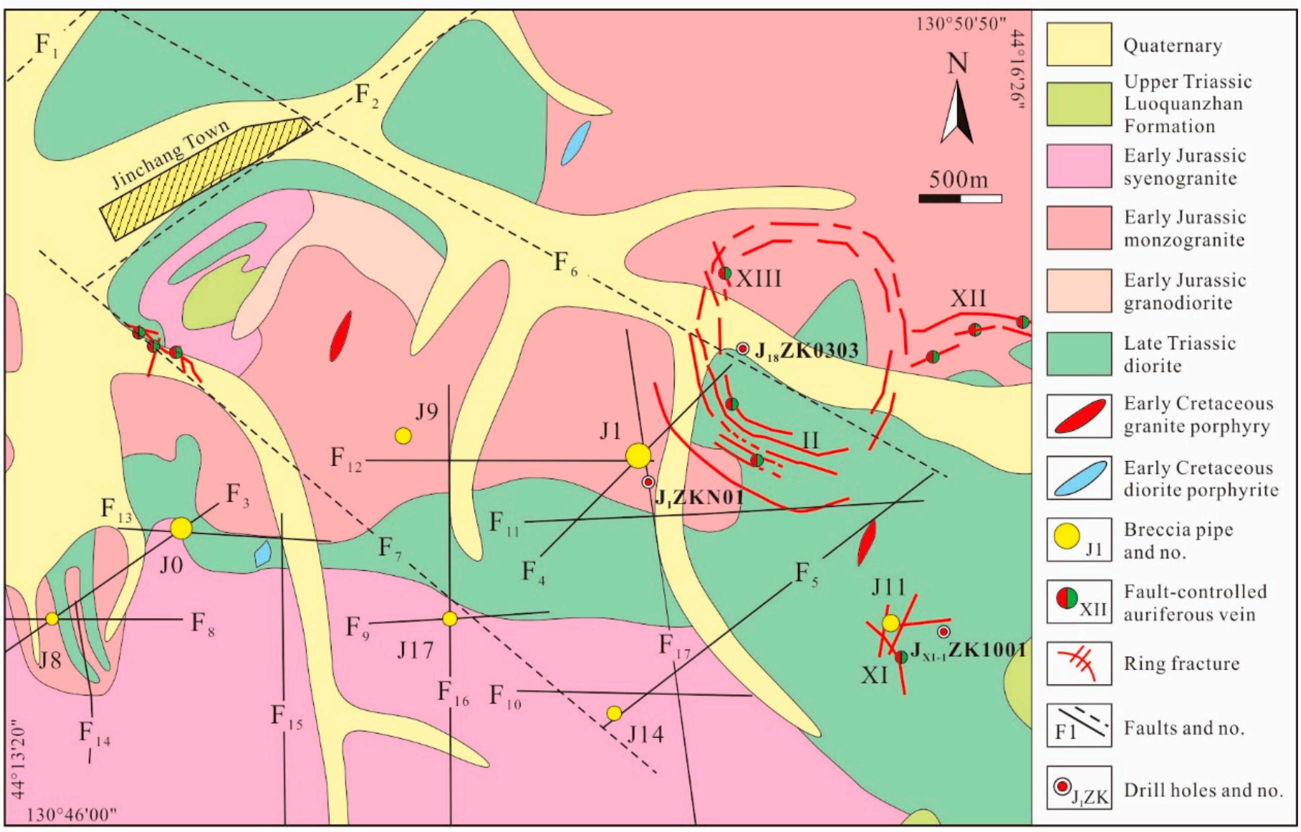

Figure 2. Geologic map of the Jinchang ore district (modified from Wang [12]).

3.2. Au Mineralization

As mentioned before, the Jinchang Au deposit displays three mineralization styles, i.e., Au-bearing breccia pipes, fault-controlled auriferous veins, and disseminated Au in granitoids [9,12,13]. Among these, the Au-bearing breccia pipes are the most important mineralization style and occur in the intersections of two sets of faults within the Early Jurassic granitoids and the Late Triassic diorite (Figure 2). At present, the Jinchang deposit contains J0, J1, J8, J9, J10, J11, J14, and J17 Au-bearing breccia pipes (Figure 2), most of which show the characteristics of large-scale, high-grade, and "full pipe" Au mineralization. The J1 Au-bearing breccia pipe is the most representative and largest Au orebody, which accounts for ~70% of the total Au resources provided by the Jinchang deposit [12]. The breccia pipe is controlled by the intersection of the F4, F12, and F17 faults within the Early Jurassic monzogranite (Figure 2), and in three dimensions, it appears as a long cylindrical body that plunges toward 160–170° at an angle of 80–85° and extends downward for ~540 m [15,32]. The average grades of the Au ores obtained from the J1 breccia pipe at the surface gradually decrease from 11.68 g/t at the center to 4.94 g/t at the edge [15,32]. The auriferous pyrites from the cement of the breccia-hosted ores yield an Re–Os isochron age of 102.9 ± 2.7 Ma, which represents the formation age of the Au-bearing J1 breccia pipe [12].

The disseminated Au mineralization occurs mainly in the concealed monzogranite beneath the ring fracture in the eastern part of the ore district (Figure 2), and was formed at

99.3 ± 7.9 Ma [12]. It appears as an Au-bearing pyrite that is controlled by the microfractures in the monzogranite. Four industrial Au orebodies have been delineated in this Au mineralization zone, namely the No. 18-1, 18-2, 18-3, and 18-4 orebodies [12,32]. A single Au orebody chiefly occurs in a stratiform-like shape that extends outward for ~800 m and has an average thickness of ~6.65 m [32].

The fault-controlled auriferous veins are the Au mineralization dominated by the auriferous sulfide-quartz veins filling the ring fracture systems within the Late Triassic diorite and Early Jurassic monzogranite (Figure 2). Four ore vein groups, namely Nos. II, III, XII, and XIII, have been discovered thus far. No. II is the representative vein group, which contains five sub-parallel-veined Au orebodies that generally have lengths in the range of 160–1600 m, average thicknesses of 0.53–1.12 m, and extend downward for 160–220 m, with average grades varying from 22.2 to 2.1 g/t Au [15]. Wang et al. [12] reported that the auriferous sulfide-quartz veins occurred at 101.2 ± 4.2 Ma in the Early Cretaceous.

3.3. Sample Descriptions

To find out the ages, magma sources, and tectonic settings of the concealed igneous intrusions and their relationships with the Au mineralization, 16 igneous rock samples from the eastern ore district were selected by the drill holes for petrography, geochemistry, zircon U–Pb dating, and Hf isotopic analysis; the locations of the drill holes are shown in Figure 2.

The samples, named as GSJ1, J1-1, J1-2, J1-3, J1-4, and J1-5, were collected from the drill hole J_IZKN01 at a depth of 670–709 m near the J1 breccia pipe (Figure 2). These samples were identified as yellowish-brown monzogranites with medium granitic textures and massive structures, mainly composed of quartz (~35%), plagioclase (~30%), alkali feldspar (~30%), biotite (~5%), and minor accessory zircon and apatite (Figure 3A).

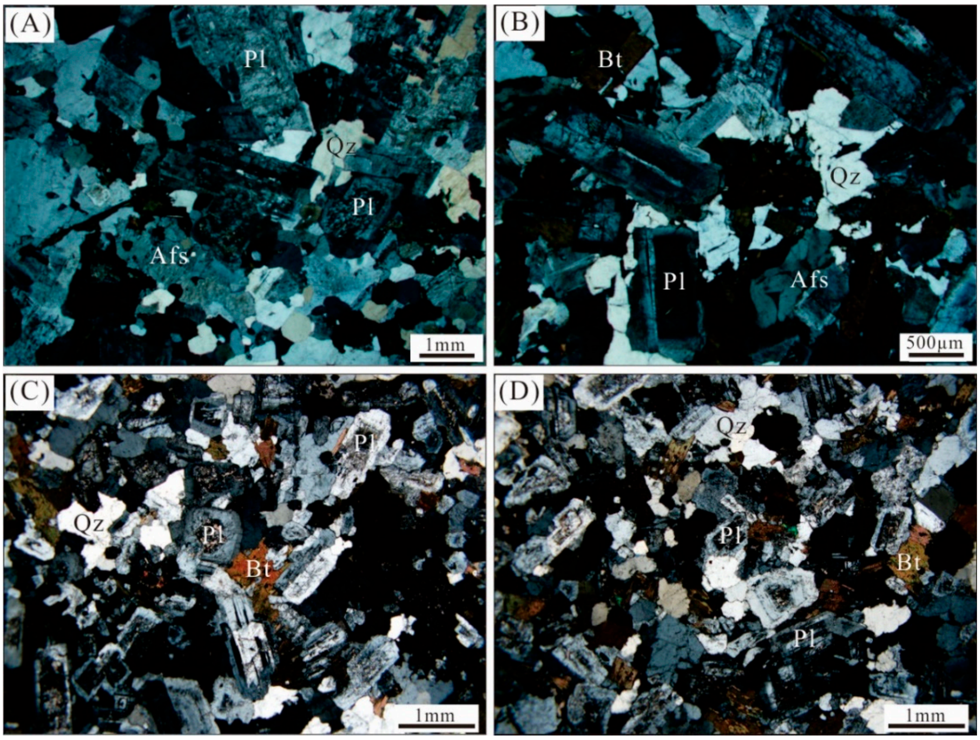

Figure 3. Representative photomicrographs (crossed polarized light) for concealed rock samples in the Jinchang ore district. (**A**) Monzogranite (sample GSJ1) from the drill hole J_IZKN01; (**B**) monzogranite (samples GSJ18) from the drill hole J_{18}ZK0303; (**C**,**D**) granodiorite (sample GSJ11) from the drill hole $J_{XI\text{-}1}$ZK1001. Abbreviations: Afs = alkali feldspar; Bt = biotite; Pl= plagioclase; Qz = quartz.

The samples GSJ18, J18-1, J18-2, J18-3, J18-4, and J18-5 belonged to a monzogranite and were collected from the drill hole J_{18}ZK0303 at a depth of 455–506 m below the surface of the No. 18 disseminated Au mineralization zone (Figure 2). The mineral compositions of these samples, similar to those of the samples from the J_IZKN01, mainly contained plagioclase (~35%), alkali feldspar (~30%), quartz (~30%), biotite (~5%), and minor accessory minerals (Figure 3B).

The samples GSJ11, 17J11-3, 17J11-4, and 17J11-5 were collected from the drill hole $J_{XI\text{-}1}$ZK1001 at a depth of 427–468 m near the J11 breccia pipe in the southeastern Jinchang ore district (Figure 2). These samples exhibited a light gray color, fine granitic textures, and massive structures, mainly consisting of plagioclase (~40%), quartz (~35%), biotite (~15%), alkali feldspar (~10%), and minor accessory minerals (Figure 3C,D) and were thus identified as fine-grained granodiorites. These are concealed intrusions beneath the Late Triassic diorite within the southeastern part of the ore district.

4. Analytical Methods

4.1. Zircon U–Pb Dating

The zircon grains were separated from the three crushed whole-rock samples GSJ1, GSJ18, and GSJ11 using the combination of conventional heavy-liquid and magnetic techniques (Supplementary Table S1). The zircons with euhedral crystals from each sample, after being handpicked under a binocular microscope, were mounted in epoxy mounts and then polished to expose their internal structures. The polishing was performed to select potential target sites for laser ablation inductively coupled plasma mass spectrometry (LA–ICP–MS) U–Pb analyses, using transmitted and reflected lights, and cathodoluminescence (CL) images. The CL images were collected using a CL spectrometer (Garton Mono CL3+) on a Quanta 200F ESEM system with 2 min scanning time under conditions of 15 kV and 120 nA beam current at the laboratory of the Sample Solution Analytical Technology Co., Ltd. in Wuhan, China. The zircon U–Pb analysis was performed using an Agilent 7500a ICP–MS equipped with a GeoLas 2005 laser ablation system at the State Key Laboratory of Geological Processes and Mineral Resources of the China University of Geosciences, Wuhan, China. The laser spot size was set to 32 μm under the operation conditions of ~10 J/cm^2 energy density and 8 Hz repetition rate, with He as the carrier gas. Zircon 91500 and silicate glass NIST 610 were used as the external reference materials for calibrating the U–Pb isotope data and trace element contents, respectively. The detailed instrument settings, analytical procedures, and data reduction were reported by Yuan et al. [33] and Liu et al. [34,35]. Concordia diagrams and weighted mean calculations were obtained using Isoplot/Ex ver. 3.0 [36]. The uncertainties in individual analyses in the data table are reported at the 1σ level; pooled ages are quoted with a 95% (2σ) confidence interval.

4.2. Whole-Rock Major and Trace Element Analyses

A total of 13 unaltered rock samples from the concealed igneous intrusions in the eastern part of the Jinchang ore district were collected by the drill holes J_IZKN01, J_{18}ZK0303, and $J_{XI\text{-}1}$ZK1001 for whole-rock geochemical analyses at the ALS Chemex (Guangzhou) Co., Ltd., Guangdong, China. The major and trace element contents, after these samples were crushed and powdered in an agate mill to ~200 mesh and were determined using X-ray fluorescence (MEXRF26) and ICP–MS, respectively (Supplementary Table S2). The analytical precision was better than 5% for the major elements and 10% for the trace elements, as estimated using the international standards BHVO-2 and BCR-2, and national standards GBW07103 and GBW07104.

4.3. Zircon Hf Isotope Analyses

After the zircon U–Pb dating, the GSJ1, GSJ18, and GSJ11 zircons were used for in situ Hf isotopic analyses using a Neptune multicollector (MC)-ICP-MS system with a 193 nm laser at the laboratory of the Tianjin Center of Geological Survey, China Geological Survey (Supplementary Table S3). The raw count rates for ^{172}Yb, ^{173}Yb, ^{175}Lu, ^{176}(Hf + Yb +Lu),

^{177}Hf, ^{178}Hf, ^{179}Hf, ^{180}Hf, and ^{182}W were simultaneously detected by nine Faraday cups. He was used as the carrier gas and was merged with Ar (makeup gas) after the ablation cell. All the data were acquired on the zircons in a single-spot ablation mode with a spot size of 50 μm and under the operating conditions of ~10 J/cm^2 energy density and 8 Hz repetition rate. Each measurement consisted of 20 s of acquisition of the background signal followed by 50 s of ablation signal acquisition. The zircon standard PLE was measured to correct and monitor the Hf isotopic values. Off-line selection and integration of the analyte signals and mass bias calibrations were performed using ICPMSDataCal [35]. The detailed analytical technique, procedures, and Hf model age calculations were described by Wu et al. [37], Griffin et al. [38], and Nowell et al. [39].

5. Analytical Results

5.1. Zircon U–Pb Dating

LA–ICP–MS zircon U–Pb data for the samples GSJ1, GSJ18, and GSJ11 are listed in Table S1 and shown in Figure 4, along with their representative zircon CL images. Zircons obtained from these samples (GSJ1, GSJ18, and GSJ11) were colorless to brown colored, transparent, and euhedral, with grain sizes generally varying from 90 to 180 μm, along with aspect ratios between 1:1 and 4:1. In the CL images, the zircon grains exhibit an obvious rhythmic oscillatory zoning. These features, combined with their high Th/U ratios of 0.31 to 1.27 (Table S1), indicate the magmatic origin of the zircons [40,41].

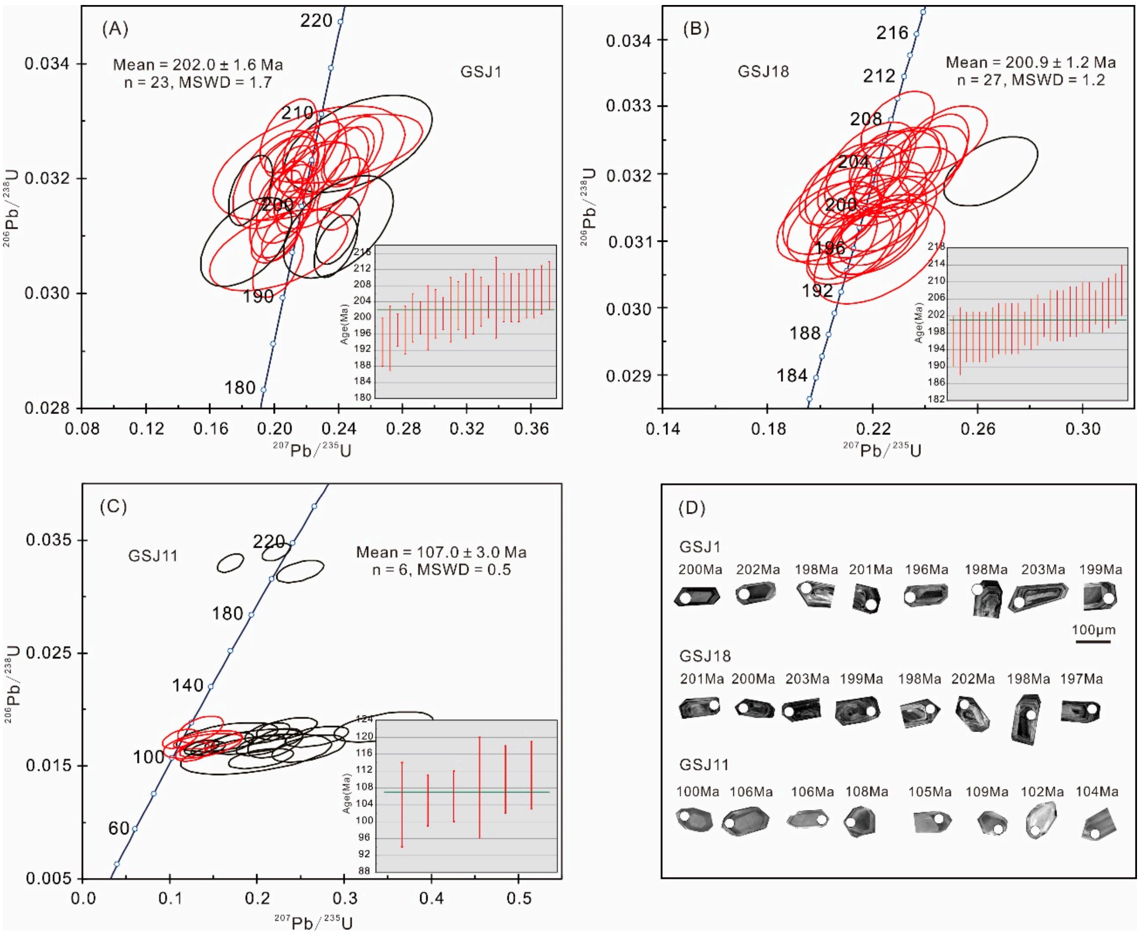

Figure 4. Zircon LA–ICP–MS U-Pb concordia diagrams (**A**–**C**) and representative zircon CL images (**D**) for the concealed rock samples GSJ1, GSJ18, and GSJ11 in the Jinchang ore district. The weighted mean age and MSWD are shown in figures (**A**–**C**).

Six analyses with high discordance degrees (>10%) among 29 spots of zircons obtained from the sample GSJ1 and the remaining 23 zircons of discordance degrees of ≤10% yielded $^{206}Pb/^{238}U$ ages of 208 to 194 Ma (Table S1). All the U–Pb data are plotted in the concordia diagram, with the > 10% discordance degree data shown in black (Figure 4A). The data for the 23 U–Pb of low discordance degrees (≤10%) have a weighted mean $^{206}Pb/^{238}U$ age of 202.0 ± 1.6 Ma (MSWD = 1.7; Figure 4A).

Data for U–Pb for the 28 samples from GSJ18 are plotted in the concordia diagram, with only one zircon with a high discordance degree (18%; GSJ18-8), marked in black (Figure 4B). The $^{206}Pb/^{238}U$ ages of 27 spots (discordance degree ≤ 10%) range from 208 to 196 Ma (Table S1), and yielded a weighted mean age of 200.9 ± 1.2 Ma (MSWD = 1.2; Figure 4B).

For the sample GSJ11, almost all the zircon U–Pb age data (111–100 Ma) exhibited a high discordance degree (>20%), except the three inherited zircons (215, 209, and 204 Ma) captured from the wall-rocks (Table S1). U–Pb data for 23 samples are plotted in the concordia diagram, with the ones of both higher (>25%) discordance degree and inherited zircons shown in black (Figure 4C). The U–Pb data for samples with a <25% discordance degree were treated as near-concordant data for the concordant age and weighted mean age calculations. Six $^{206}Pb/^{238}U$ ages of a discordance degree of <25% are concentrated in the interval of 111 to 104 Ma. They yielded a concordant age of 104.0 ± 3.7 Ma, which coincides with the errors with a weighted mean $^{206}Pb/^{238}U$ age of 107.0 ± 3.0 Ma (MSWD = 0.5; Figure 4C).

5.2. Major and Trace Element Geochemistry

The major and trace element analytical data for 13 rock samples collected from the drill holes J_IZKN01, $J_{18}ZK0303$, and $J_{XI\text{-}1}ZK1001$ from the concealed igneous intrusions in the Jinchang ore district are listed in Table S2. The monzogranite samples from the drill holes J_IZKN01 and $J_{18}ZK0303$ have similar geochemical features and contain higher SiO_2 contents of 71.03–72.91 wt%, Al_2O_3 contents of 13.02–13.94 wt%, MgO contents of 0.35–0.43 wt%, Fe_2O_3 contents of 2.36–3.10 wt%, and a total $Na_2O + K_2O$ content of 6.75–7.90 wt%, with the A/CNK values of 0.99–1.07 (Table S2). Geochemically, these rock samples are classified as high- to medium-K calc-alkaline series on the K_2O vs. SiO_2 diagram (Figure 5A) and show weakly peraluminous features on the A/NK vs. A/CNK diagram (Figure 5B). They have total rare-earth element (REE) abundances ranging from 113 to 147 ppm (Table S2) and are enriched in light rare-earth elements (LREEs) and large-ion lithophile elements (LILEs; e.g., Rb, Th, U, and K) but are relatively depleted in heavy rare-earth elements (HREEs) and high field strength elements (HFSEs; e.g., Nb, Ta, and Ti), P, and Sr, with negative Eu anomalies (Figure 6A,B).

The granodiorite samples from the drill hole $J_{XI\text{-}1}ZK1001$ contain an SiO_2 content of 65.57–67.73 wt%, Al_2O_3 content of 14.57–16.14 wt%, MgO content of 1.42–1.57 wt%, Fe_2O_3 content of 4.69–5.52 wt%, and a total $Na_2O + K_2O$ content of 5.90–7.56 wt% (Table S2). They are classified as the medium-K calc-alkaline series on the K_2O vs. SiO_2 diagram (Figure 5A) and belong to the metaluminous to weakly peraluminous granites on the A/NK vs. A/CNK diagram (Figure 5B). Similarly, the trace element compositions of these samples are characterized by the enrichment of the LREEs and LILEs (e.g., Rb, Ba, Th, U, and K) and the depletion of the HREEs, HFSEs (e.g., Nb, Ta, and Ti), and P (Figure 6C,D).

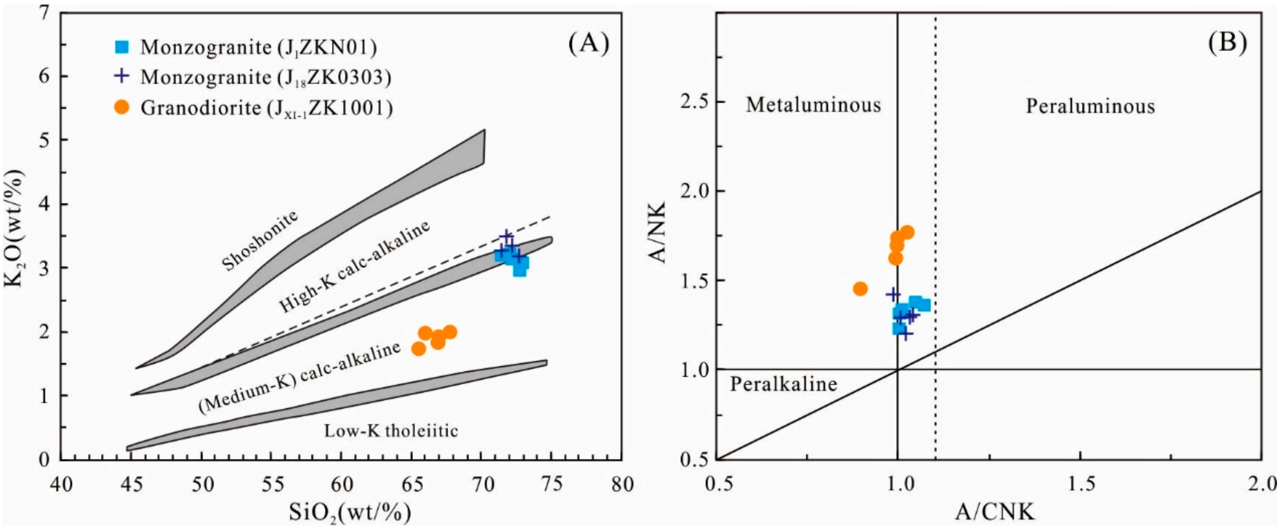

Figure 5. Plots of (**A**) K_2O vs. SiO_2 (after Peccerillo and Taylor [42]) and (**B**) A/NK [molar ratio $Al_2O_3/(Na_2O + K_2O)$] vs. A/CNK [molar ratio $Al_2O_3/(CaO + Na_2O + K_2O)$] (after Maniar and Piccoli [43]) for the concealed granitoids in the Jinchang ore district. Data of two granodiorite samples are quoted from Cai et al. [9].

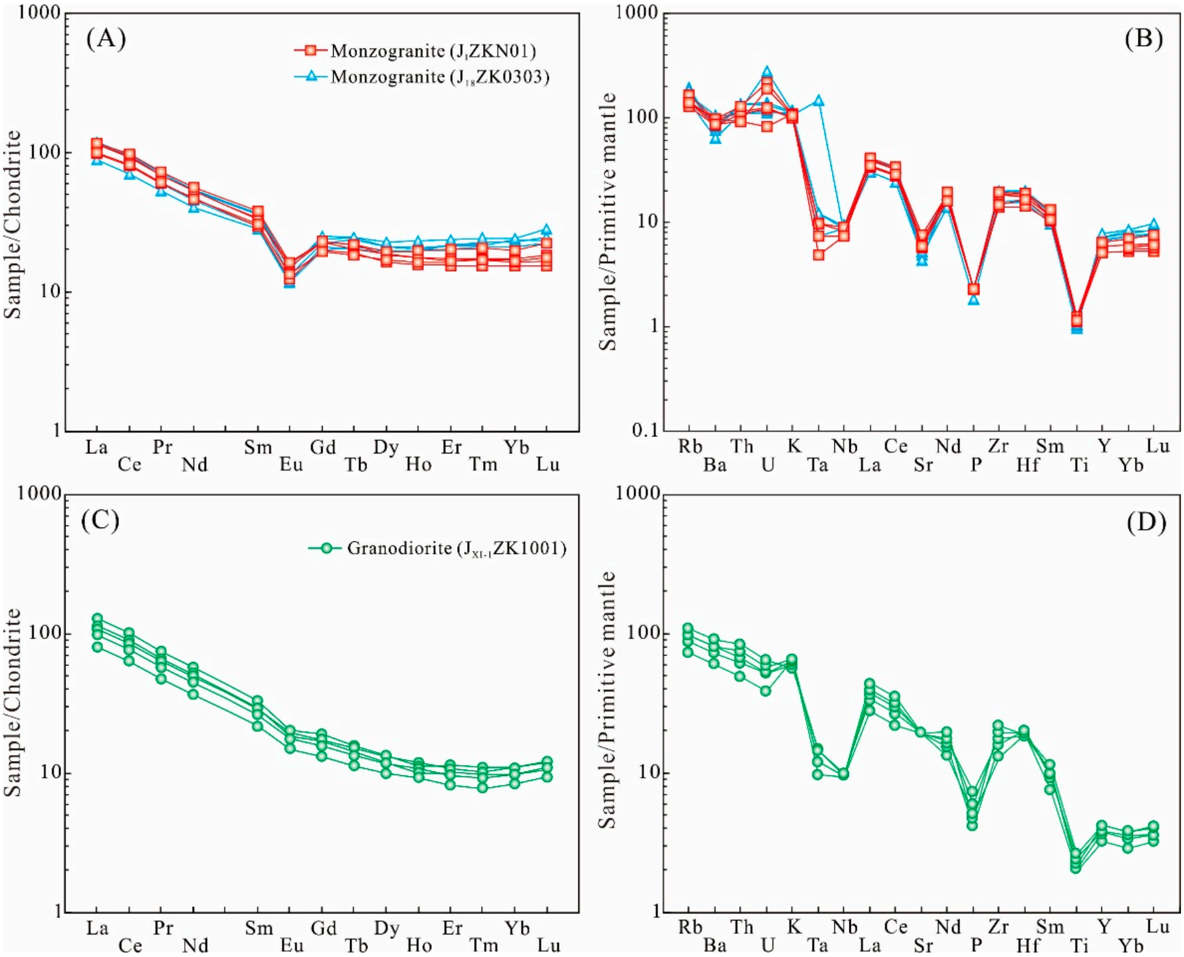

Figure 6. Chondrite-normalized REE patterns (**A**,**C**) and primitive mantle (PM) normalized trace element (**B**,**D**) diagrams for the concealed granitoids in the Jinchang ore district. Normalizing values are from Sun and McDonough [44]. Data of two granodiorite samples are quoted from Cai et al. [9].

5.3. Zircon Hf Isotopes

In this study, we focused on the primary zircons that were formed from magma crystallization. Inherited zircons, captured from the wall-rocks, were not used for work on Hf isotopic analysis. The in situ Hf isotopic results of the zircons obtained from the samples GSJ1, GSJ18, and GSJ11 are presented in Table S3 and Figure 7. The $^{176}Hf/^{177}Hf$ ratios and εHf(t) values of the zircons obtained from the sample GSJ1 range from 0.282850 to 0.282960 and +7.1 to +10.9, respectively, with the two-stage model ages (T_{DM2}) of 712 to 500 Ma (Table S3). Additionally, sample GSJ18 exhibits similar $^{176}Hf/^{177}Hf$ ratios of 0.282808 to 0.282969, εHf(t) values of +5.6 to +11.2, and T_{DM2} of 799 to 481 Ma (Table S3). The zircons from sample GSJ11 yielded $^{176}Hf/^{177}Hf$ ratios of 0.282833 to 0.283037 and εHf(t) values of +4.4 to +11.5, with T_{DM2} ranging from 787 to 389 Ma (Table S3).

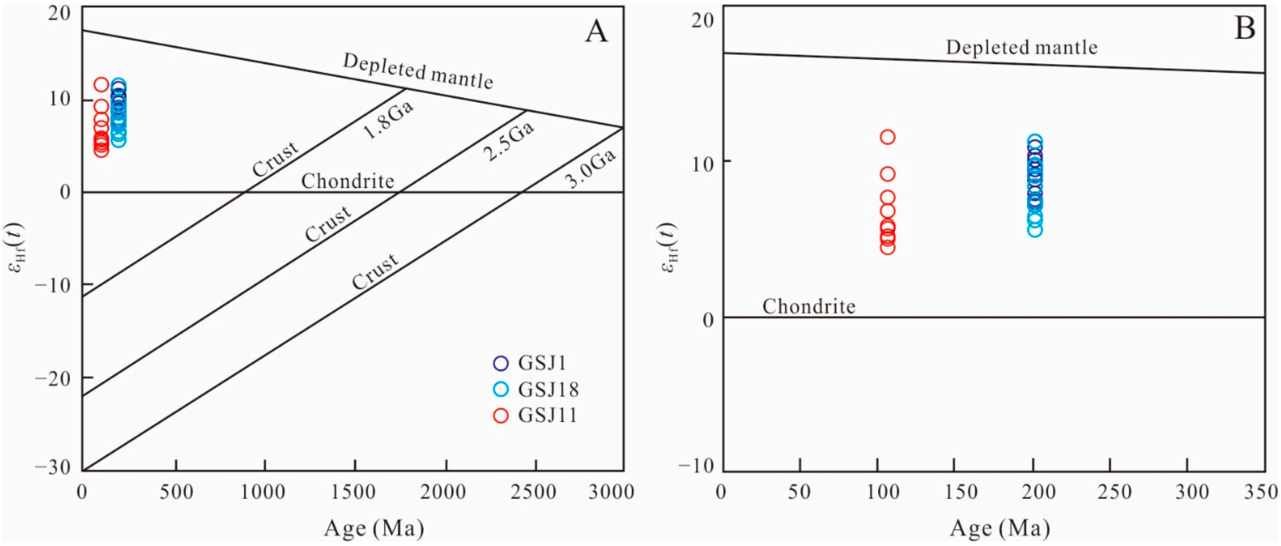

Figure 7. (**A**) Plots of zircon εHf(t) vs. T (Ma) for the concealed granitoids in the Jinchang ore district. (**B**) Close-up view of the distribution of samples in Figure 7A.

6. Discussion

6.1. Magma Sources

Two concealed monzogranites (GSJ1 and GSJ18) yielded zircon U–Pb ages of 202.0 ± 1.6 and 200.9 ± 1.2 Ma, respectively (Figure 4A,B), which represent the crystallization ages of the monzogranites at a depth of 670–709 m near the J1 breccia pipe and 455–506 m beneath the surficial ring fracture systems within the disseminated Au mineralization zone (Figure 2). These crystallization ages of the monzogranites are consistent with the those of the large-scale ore-hosting granitoid wall-rocks exposed in the Jinchang ore district (206–185 Ma) [25,29–31] but are obviously earlier than the Early Cretaceous Au mineralization (114–100 Ma) [9,13,14]. This suggests that the Au mineralization was not genetically associated with the monzogranite. The dating results of the monzogranites (Figure 4A,B), combined with their similar geochemical and Hf isotopic compositions (Tables S2 and S3; Figures 5–7), indicate that they are cogenetic. The monzogranite samples have much higher Rb/Sr (0.55–1.32), La/Nb (3.54–5.21), Th/Nb (1.48–1.86), and Th/La (0.29–0.49) ratios (Table S2) compared to the average ratios of the mantle (Rb/Sr: 0.030; La/Nb: 0.94; Th/Nb: 0.117; Th/La: 0.125) [44,45]. Moreover, the low $Mg^{\#}$ values (19.68–24.66) for the monzogranites support a crustal ($Mg^{\#} < 40$) rather than mantle magma source [46]. Furthermore, the zircons of the monzogranites yielded positive εHf(t) values of +5.6 to +11.2 (Figure 7) with the T_{DM2} of 799 to 481 Ma (Table S3), which indicates the absence of the contribution of any ancient continental crust materials (older than ca. 1000 Ma) [47]. Collectively, these data show that the Early Jurassic monzogranite was derived from the partial melting of the Neoproterozoic–Paleozoic continental crust.

The zircons from the concealed granodiorite (GSJ11) yielded a U–Pb age of 107.0 ± 3.0 Ma (Figure 4C), which is interpreted as the crystallization age of the granodiorite at a depth of 427–468 m near the J11 breccia pipe (Figure 2). Previous studies suggested that the Au mineralization of the Jinchang deposit occurred in the Early Cretaceous (ca. 114–100 Ma), and the ore materials were mainly sourced from the magmatic fluids closely related to the fractional crystallization of monzonite and granodiorite [9,13,48]. The concealed granodiorite samples were found to contain many disseminated sulfides, including pyrite and sphalerite (Figure 8), and exhibited significantly higher metal contents compared to the Early Jurassic barren monzogranite. This, combined with the crystallization age of 107.0 ± 3.0 Ma for the granodiorite, supports concealed Early Cretaceous granodiorite as the ore-causative rock for the Au mineralization at Jinchang. The Early Cretaceous granodiorite yielded lower Rb/Sr (0.11–0.17), Th/Nb (0.63–1.04) and Th/La (0.22–0.23) ratios and higher $Mg^{\#}$ values (34.07–39.87) than those of the Early Jurassic monzogranites (Table S2). These Rb/Sr, Th/Nb and Th/La ratios and $Mg^{\#}$ values move toward the average mantle composition [44,45,49]. Some mafic microgranular enclaves occur in the granodiorite (Figure 8b) and are most likely linked to the mantle materials [5,19]. A combination of the trace elemental ratios, petrographic feature, and εHf(t) values (+4.4 to +11.5) with the T_{DM2} of 787 to 389 Ma (Table S3; Figure 7) indicate that the mixture of the Neoproterozoic–Paleozoic continental crust and mantle materials may have provided magmas for the granodiorite. Additionally, we cannot ignore the sources of the sulfide minerals deposited from ore-bearing magmatic fluids related to the fractional crystallization of the granodiorite. Mao et al. [50] suggested that the Re abundance in molybdenite decreases when going from a mantle source to mixtures between the mantle and the crust, and then to crust, with the mantle-derived Re abundances as high as 171 to 1280 ppm. The molybdenites in the Au ores at Jinchang have high Re abundances, ranging from 241 to 410 ppm [9,12], reflecting an upper-mantle source for the molybdenite. Moreover, 15 auriferous pyrites from the J1 breccia pipe, the fault-controlled veins, and the No. 18 orebody yielded an average initial $^{187}Os/^{188}Os$ value of 0.71 ± 0.23 [12]. This value is higher than the initial $^{187}Os/^{188}Os$ values of the various materials obtained from the mantle (0.105–0.152) [51], but much lower than those of the continental crust (average value: 3.63) [52], indicating that the Fe and Au may have been derived from the mixture of the mantle with some continental crust materials. Furthermore, the whole-rock I_{Sr} and εNd(t) values of the coeval porphyritic diorites in the Jinchang ore district range from 0.70472 to 0.70516 and 1.8 to 2.5, respectively [15], revealing that the rock-forming materials originated from the upper mantle [53]. Finally, combined with the petrographic, element geochemical, and isotopic results, we conclude that the Early Cretaceous ore-causative granodiorite had mixed magma sources that originated from the partial melting of both the Neoproterozoic–Paleozoic continental crust and upper mantle materials. The upper mantle contributed significantly to the sources of the ore-forming materials (such as Fe, Au, and Cu) in the Early Cretaceous magmas that formed the granodiorite.

6.2. Tectonic Setting and Implications for Au Metallogeny

The monzogranite samples from the eastern Jinchang ore district belonged to the high-to medium-K calc-alkaline series of the weakly peraluminous granites (Figure 5A,B), similar to those of the igneous rocks in the active continental margins [6,8,20,54]. Moreover, all the samples can be plotted into the field of the volcanic arc granites on the granite tectonic discrimination diagrams (Figure 9A–D), which suggests that these rocks were linked to the magmatic arc setting. Based on the studies of the Early-Middle Jurassic calc-alkaline volcanic rock assemblage and the coeval bimodal igneous rock assemblage in the eastern margin of Northeast China, Xu et al. [8] demonstrated the subduction of the Paleo-Pacific Plate beneath the Eurasia in the Early-Middle Jurassic. Thus, we infer that the Early Jurassic monzogranite in the Jinchang ore district formed in the continental arc setting related to the Paleo-Pacific subduction.

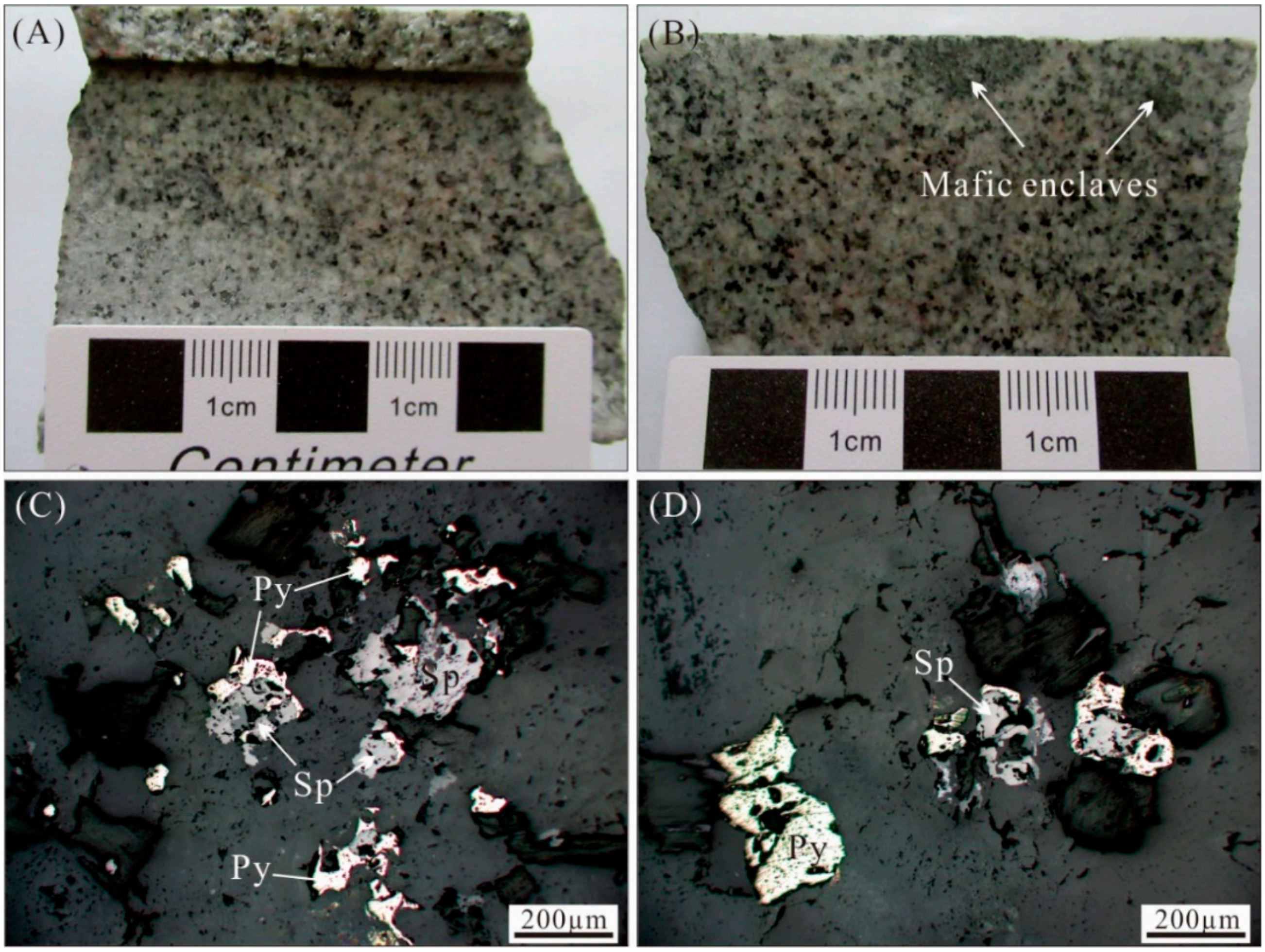

Figure 8. Photographs (**A**,**B**) and photomicrographs (**C**,**D**) of representative ore-causative granodiorite from the drill hole J_{XI-1}ZK1001, showing disseminated pyrite and sphalerite and mafic microgranular enclaves. Abbreviations: Py = pyrite; Sp = sphalerite.

The granodiorite samples were enriched in LILEs and LREEs, depleted in HREEs and HFSEs (Figure 6C,D), and classified as medium-K calc-alkaline series of metaluminous to weakly peraluminous granites (Figure 5A,B). These samples, combined with the coeval monzonites [9], plot into the field of the volcanic arc granites (Figure 9A–D). These geochemical features are indicative of the formation of the Early Cretaceous granodiorite in the continental arc setting. According to previous studies, the widespread Early Cretaceous magmatic rocks with an eastward younging trend in Northeast China were formed in the extensional setting of the back-arc area [6,19,57–59] and are interpreted to reflect the rollback of the subducted Paleo-Pacific slab [6,9,14,19,47,60–63]. Considering the ore-causative granodiorite at Jinchang from the crust–mantle mixed magmas, we infer that the Early Cretaceous subducted slab rollback most likely caused the partial melting of both the mantle wedge and overlying continental crust through fluid release, which is supported by the following points. (1) No anomalies for the ore-causative granodiorites with the precipitation of abundant metal minerals, including pyrite, magnetite, chalcopyrite, and galena [9,12–15,48] reflect that the separation of the plagioclase as residue phases in the source was insignificant, with the metals being mainly enriched in the magmatic fluids. This is most likely attributed to the water-rich magma sources [64]. (2) The granodiorite samples fall near the range of fluid metasomatism on the Nb/Y vs. La/Yb and Ba/Yb vs. Nb/Yb diagrams (Figure 10A,B), which indicates that the formation of the magmas was related to the fluid metasomatism in the source area. Based on this these combined points, we propose that the Early Cretaceous ore-causative granodiorite of the Au mineralization at Jinchang was formed in the continental arc setting. Additionally, this Early Cretaceous ore-causative granodiorite was derived from the partial melting of the mantle wedge and the overlying Neoproterozoic–Paleozoic continental crust, which was possibly caused by the dehydration and metasomatism of the subducted Paleo-Pacific slab involved in the rollback (Figure 11). The geodynamic setting of the subducted slab rollback supported the widespread Early Cretaceous magmatic–hydrothermal Au mineralization, not only for the Jinchang Au deposit, which formed in the continental arc environment, but for all the other coeval hydrothermal Au deposit formations in the Yanbian–Dongning region in Northeast China, including the Xiaoxi'nancha, Naozhi, Ciweigou, and Jiusangou Au deposits (Figures 1B and 11).

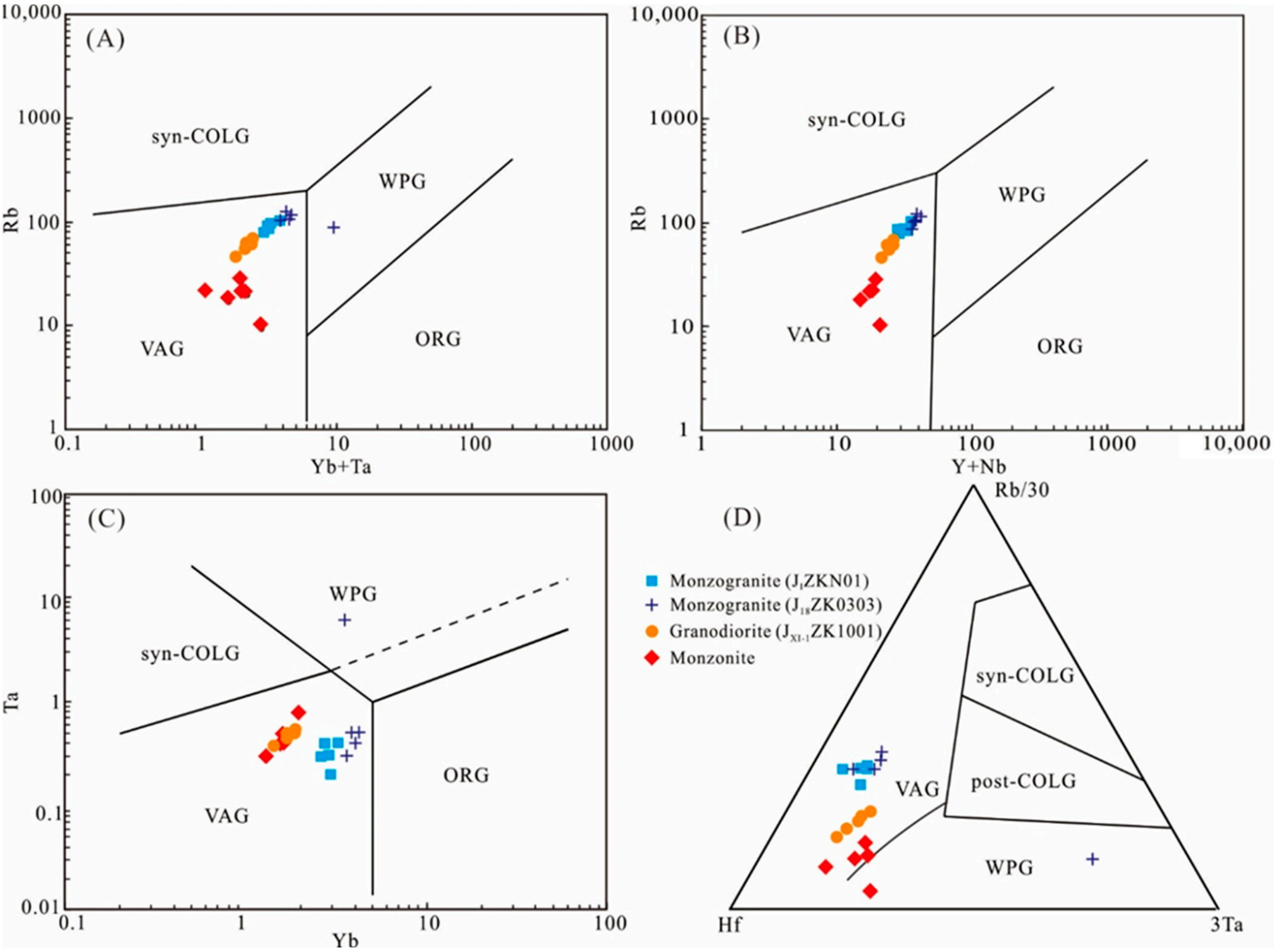

Figure 9. Tectonic discrimination diagrams for the granitoids in the Jinchang ore district. (**A**) Rb vs. (Yb + Ta); (**B**) Rb vs. (Y + Nb); (**C**) Ta vs. Yb (after Pearce et al. [55]). (**D**) Ternary (Rb/30)-Hf-(Ta×3) (after Harris et al. [56]). The data from the monzonites and two granodiorites are quoted from Cai et al. [9]. Abbreviations: VAG = volcanic arc granites; ORG = ocean ridge granites; WPG = within-plate granites; syn-COLG = syn-collision granites; post-COLG = post-collision granites.

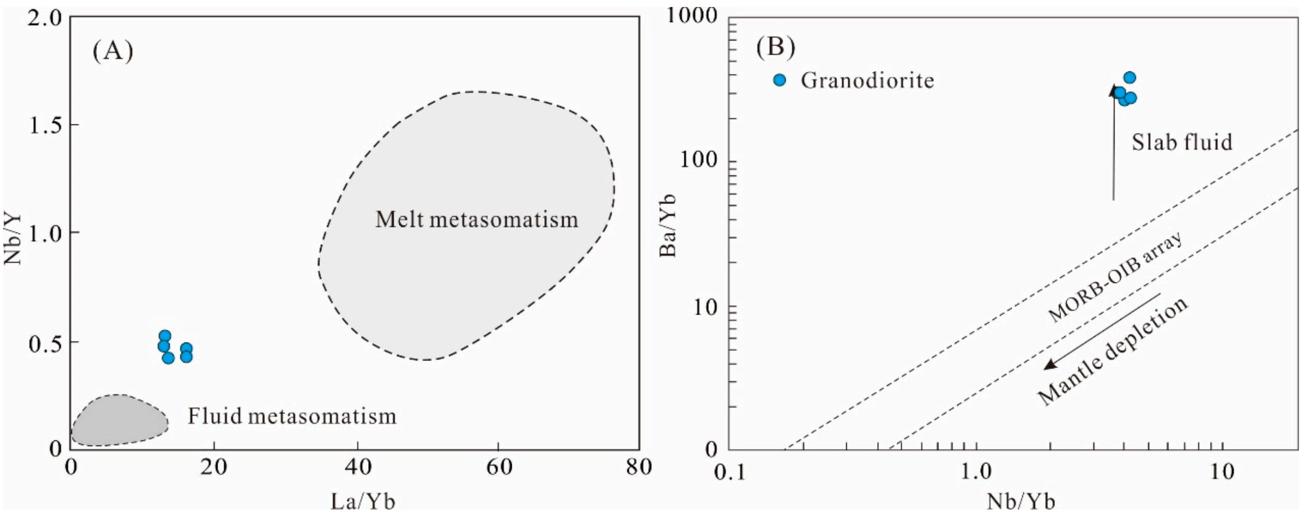

Figure 10. Plots of (**A**) Nb/Y vs. La/Yb (after Hoffer et al. [65]) and (**B**) Ba/Yb vs. Nb/Yb (after Chen et al. [66]).

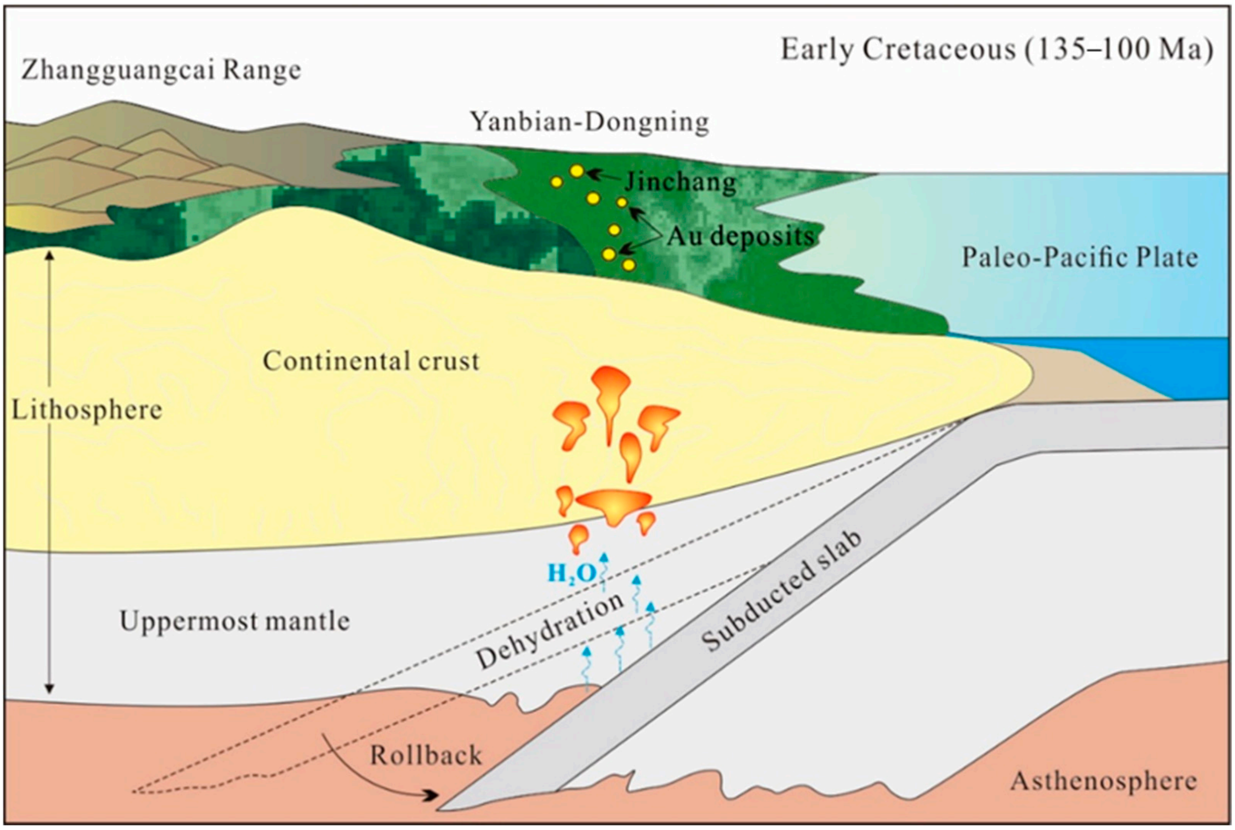

Figure 11. Schematic diagram illustrating a proposed genetic model and geodynamic setting for the Early Cretaceous granodiorite at Jinchang in the Yanbian–Dongning Region, NE China.

7. Conclusions

(1) The zircon U–Pb dating results indicated that the crystallization ages of the concealed monzogranites (GSJ1 and GSJ18) near the J1 auriferous breccia pipe and the No. 18 disseminated Au mineralization in the Jinchang ore district are 202.0 ± 1.6 and 200.9 ± 1.2 Ma, respectively. The concealed granodiorite near the J11 auriferous breccia pipe yielded a younger crystallization age of 107.0 ± 3.0 Ma.

(2) The Early Jurassic monzogranite was derived from the partial melting of the Neoproterozoic–Paleozoic continental crust, whereas the Early Cretaceous granodiorite originated from the mixing magmas of the mantle wedge and the overlying continental crust.
(3) The Early Jurassic ore-hosting monzogranite was formed in the continental arc setting related to the Paleo-Pacific subduction. In contrast, the formation of the ore-causative granodiorite was most likely related to the dehydration and metasomatism of the subducted Paleo-Pacific slab involved in the rollback in the Early Cretaceous.

Supplementary Materials: The following supporting information can be downloaded at: https://www.mdpi.com/article/10.3390/min12060708/s1, Table S1: LA–ICP–MS zircon U–Pb data of the concealed monzogranites (GSJ1 and GSJ18) and granodiorite (GSJ11) from the Jinchang ore district; Table S2: Major (wt.%) and trace element (ppm) contents of the concealed granitoids in the Jinchang ore district; Table S3: Zircon Hf isotope data of the concealed granitoids in the Jinchang ore district.

Author Contributions: Conceptualization, Z.W., W.C. and S.L.; software, S.L. and W.C.; investigation, Z.W., W.C. and S.L.; data curation, X.M.; funding acquisition, Z.W.; project administration, Z.W.; writing—original draft preparation, Z.W.; writing—review and editing, Z.W. and W.C. All authors have read and agreed to the published version of the manuscript.

Funding: This research was funded by the National Natural Science Foundation of China (42102074), the China Geological Survey (WT202006), and the Education Department of Jilin Province (JJKH2000608KJ).

Acknowledgments: We would like to thank Liang Chang and Yong Cao from the Mudanjiang Comprehensive Survey Center of Natural Resources, China Geological Survey, for their help with field work. We also thank the anonymous reviewers for the detailed and constructive comments that greatly improved the manuscript.

Conflicts of Interest: The authors declare no conflict of interest.

References

1. Xiao, W.J.; Windley, B.F.; Hao, J.; Zhai, M.G. Accretion leading to collision and the Permian Solonker suture, Inner Mongolia, China: Termination of the central Asian orogenic belt. *Tectonics* **2003**, *22*, 1069–1088. [CrossRef]
2. Jia, D.C.; Hu, R.Z.; Lu, Y.; Qiu, X.L. Collision belt between the Khanka block and the North China block in the Yanbian Region, Northeast China. *J. Asian Earth Sci.* **2004**, *23*, 211–219.
3. Zhang, Y.B.; Wu, F.Y.; Wilde, S.A.; Zhai, M.G.; Lu, X.P.; Sun, D.Y. Zircon U–Pb ages and tectonic implications of "Early Paleozoic" granitoids at Yanbian, Jilin Province, NE China. *Isl. Arc* **2004**, *13*, 484–505. [CrossRef]
4. Li, J.Y. Permian geodynamic setting of Northeast China and adjacent regions: Closure of the Paleo-Asian Ocean and subduction of the Paleo-Pacific Plate. *J. Asian Earth Sci.* **2006**, *26*, 207–224. [CrossRef]
5. Yang, J.H.; Wu, F.Y.; Shao, J.A.; Wilde, S.A.; Xie, L.W.; Liu, X.M. Constraints on the timing of uplift of the Yanshan Fold and Thrust Belt, North China. *Earth Planet. Sci. Lett.* **2006**, *246*, 336–352. [CrossRef]
6. Wu, F.Y.; Sun, D.Y.; Ge, W.C. Geochronology of the Phanerozoic granitoids in northeastern China. *J. Asian Earth Sci.* **2011**, *41*, 1–30. [CrossRef]
7. Liu, S.; Hua, R.Z.; Gao, S.; Feng, C.X.; Coulsonc, I.M.; Feng, G.Y.; Qi, Y.Q.; Yang, Y.H.; Yang, C.G.; Tang, L. Zircon U–Pb age and Sr–Nd–Hf isotopic constraints on the age and origin of Triassic mafic dikes, Dalian area, Northeast China. *Int. Geol. Rev.* **2013**, *55*, 249–262. [CrossRef]
8. Xu, W.L.; Wang, F.; Pei, F.P.; Meng, N.; Tang, J.; Xu, M.J.; Wang, W. Mesozoic tectonic regimes and regional ore-forming background in NE China: Constraints from spatial and temporal variations of Mesozoic volcanic rock associations. *Acta Petrol. Sin.* **2013**, *29*, 339–353. (In Chinese with English Abstracrt)
9. Cai, W.Y.; Wang, Z.G.; Li, J.; Fu, L.J.; Wang, K.Y.; Konare, Y. Zircon U-Pb and molybdenite Re-Os geochronology and geochemistry of Jinchang porphyry gold-copper deposit, NE China: Two-phase mineralization and the tectonic setting. *Ore Geol. Rev.* **2019**, *107*, 735–753. [CrossRef]
10. Ren, Y.S.; Chen, C.; Zou, X.T.; Zhao, H.L.; Hao, Y.J.; Hou, H.N.; Hu, Z.C.; Jia, G.H. The age, geological setting, and types of gold deposits in the Yanbian and adjacent areas, NE China. *Ore Geol. Rev.* **2016**, *73*, 284–297. [CrossRef]
11. Chai, P.; Sun, J.; Xing, S.; Men, L.; Han, J. Early Cretaceous arc magmatism and high-sulphidation epithermal porphyry Cu–Au mineralization in Yanbian area, Northeast China: The Duhuangling example. *Int. Geol. Rev.* **2014**, *57*, 1267–1293. [CrossRef]

12. Wang, Z.G. Mineralization and Metallogenic Prediction of the Jinchang Cu-Au Deposit in Dongning, Heilongjiang Province. Ph.D. Thesis, Jilin University, Changchun, China, 2018. (In Chinese)
13. Li, S.D.; Wang, Z.G.; Wang, K.Y.; Cai, W.Y.; Peng, D.W.; Xiao, L.; Li, J. Re-Os Pyrite Geochronological Evidence of Three Mineralization Styles within the Jinchang Gold Deposit, Yanji-Dongning Metallogenic Belt, Northeast China. *Minerals* **2018**, *8*, 448. [CrossRef]
14. Shi, K.T.; Wang, K.Y.; Yu, H.J.; Wang, Z.G.; Ma, X.L.; Bai, X.J.; Wang, R. The $^{40}Ar/^{39}Ar$ dating of quartz: New insights into the metallogenic chronology of the Jinchang gold deposit and its geological significance. *Sci. Rep.* **2018**, *8*, 13879. [CrossRef] [PubMed]
15. Zhao, Y.S. Porphyry Gold System of the Jinchang Camp in the Yanbian-Dongning Metallogenic Belt, NE China. Ph.D. Thesis, China University of Geosciences, Beijing, China, 2013. (In Chinese)
16. Wang, Z.G.; Wan, D.; Wang, K.Y.; Konare, Y.; Liang, Y.H. Isotope systematics and fluid inclusion studies of the Hongtaiping Cu–Pb–Zn deposit in Yanbian, NE China: Implications for ore genesis. *Geol. J.* **2020**, *55*, 6912–6935. [CrossRef]
17. Tang, K.D.; Shao, J.A.; Li, J.C.; Kang, Z. Nature of the Yanbian suture zone and structure of Northeast Asian. *Geol. Bull. China* **2004**, *23*, 885–891. (In Chinese with English Abstract)
18. Zhang, C. The Mesozoic Tectonic Evolution of Yanbian Area in the Eastern Segment of Northern Margin of the North China Block. Ph.D. Thesis, Jilin University, Changchun, China, 2014. (In Chinese)
19. Wu, F.Y.; Sun, D.Y.; Lin, Q. Petrogenesis of the Phanerozoic granites and crustal growth in Northeast China. *Acta Petrol. Sin.* **1999**, *15*, 181–189. (In Chinese with English Abstract)
20. Cao, H.H.; Xu, W.L.; Pei, F.P.; Wang, Z.W.; Wang, F.; Wang, Z.J. Zircon U–Pb geochronology and petrogenesis of the Late Paleozoic–Early Mesozoic intrusive rocks in the eastern segment of the northern margin of the North China Block. *Lithos* **2013**, *170–171*, 191–207. [CrossRef]
21. Zhang, Y.B.; Wu, F.Y.; Wilde, S.A.; Zhai, M.G.; Lu, X.P.; Zhang, X.F. Geochronology and Tectonic Implications of the "Proterozoic" Seluohe Group at the Northern Margin of the North China Craton. *Int. Geol. Rev.* **2008**, *50*, 135–153. [CrossRef]
22. Zhang, Y.B.; Wu, F.Y.; Sun, D.Y.; Li, H.M. Single grain zircon U–Pb ages of the "Early Hercynian" Miantian granites and Zhongping hypersthene diorite in the Yanbian area. *Geol. Rev.* **2002**, *48*, 424–429. (In Chinese with English Abstract)
23. Wang, Z.W.; Pei, F.P.; Xu, W.L.; Cao, H.H.; Wang, Z.J.; Zhang, Y. Tectonic evolution of the eastern Central Asian Orogeni Belt: Evidence from zircon U-Pb-Hf isotopes and geochemistry of early Paleozoic rocks in Yanbian region, NE China. *Gondwana Res.* **2016**, *28*, 334–350. [CrossRef]
24. Shan, P.F.; Cao, M.J.; Jourdan, F.; Evans, N.; Ge, X.; Sun, J.G.; Qin, K.Z.; Zhao, C. Biotite $^{40}Ar/^{39}Ar$ dating and chemical composition inform metallogenesis of Xiaoxi'nancha porphyry Au-Cu deposit, NE China. *Ore Geol. Rev.* **2021**, *134*, 104140. [CrossRef]
25. Han, S.J.; Yang, Y.C.; Ye, S.Q.; Khomich, V.G.; Boriskina, N.G.; Wang, X.Y. U–Pb zircon and geochemical constraints on age and genesis ofgranitoids from the Jinchang Au deposit in Heilongjiang, NE China. *Geol. J.* **2018**, *53*, 600–616. [CrossRef]
26. Zhao, Y.J.; Sun, J.G.; Wang, Q.H.; Men, L.J.; Li, Y.X.; Guo, J.; Cui, P.L. $^{40}Ar/^{39}Ar$ laser probe dating and discussion on metallogenic epoch of epithermal Au-Cu deposit in Yanbian area of Jilin. *Earth Sci. Front.* **2010**, *17*, 156–169. (In Chinese with English abstract)
27. Men, L.J. An Ore-forming Fluid Study on Late Mesozoic Epithermal Au–Cu Deposit in Yanbian-Dongning Area: Implication for the Metallogenic Mechanism. Ph.D. Thesis, Jilin University, Changchun, China, 2011. (In Chinese)
28. Men, L.J.; Sun, J.G.; Zhao, J.K.; Chen, L.; Liang, S.N.; Pang, W.; Chen, D. Fluidinclusions in breccia type copper gold ore bodies of Jinchang gold deposit, Dongning county, Heilongjiang province. *Miner. Depos.* **2008**, *27*, 71–80. (In Chinese with English abstract)
29. Zhang, H.F.; Li, S.R.; Santosh, M.; Liu, J.J.; Diwu, C.R.; Zhang, H. Magmatism and metallogeny associated with mantle upwelling: Zircon U-Pb and Lu–Hf constraints from the gold-mineralized Jinchang granite, NE China. *Ore Geol. Rev.* **2013**, *54*, 138–156. [CrossRef]
30. Lu, Y.H.; Zhang, Y.; Lai, Y.; Wang, Y.Z. LA–ICP–MS zircon U-Pb dating of magmatism and mineralization in the Jinchang gold ore-field, Heilongjiang province. *Acta Petrol. Sin.* **2009**, *25*, 2902–2912. (In Chinese with English Abstract)
31. Ma, F. Study on the Enrichment Regularity of Mineralization of Jinchang Gold Deposit, Dongning in Heilongjiang Province. Ph.D. Thesis, Jilin University, Changchun, China, 2014. (In Chinese)
32. Xu, W.X. Geological Characters, Metallogenic Regularity and Model of the Gold (Copper) Ore Fields in Jinchang, Heilongjiang province. Ph.D. Thesis, China University of Geosciences, Beijing, China, 2009. (In Chinese)
33. Yuan, H.L.; Gao, S.; Liu, X.M. Accurate U-Pb age and trace element determinations of zircon by laser ablation inductively coupled plasma mass spectrometry. *Geostand. Geoanal. Res.* **2004**, *28*, 353–370. [CrossRef]
34. Liu, Y.S.; Hu, Z.C.; Gao, S.; Günther, D.; Xu, K.J.; Gao, C.G.; Chen, H.H. In situ analysis of major and trace elements of anhydrous minerals by LA-ICP-MS without applying an internal standard. *Chem. Geol.* **2008**, *257*, 34–43. [CrossRef]
35. Liu, Y.S.; Gao, S.; Hu, Z.C.; Gao, C.G.; Zong, K.Q.; Wang, D.B. Continental and oceanic crust recycling-induced melt-peridotite interactions in the Trans-North China Orogen: U-Pb dating, Hf isotopes and trace elements in zircons from mantle xenoliths. *J. Petrol.* **2010**, *51*, 537. [CrossRef]
36. Ludwig, K.R. User's manual for Isoplot/EX version 3.0: A geochronologicaltoolkit for Microsoft Excel. *Berkeley Geochronol. Cent. Spec. Publ.* **2003**, *4*, 70.

37. Wu, F.Y.; Yang, Y.H.; Xie, L.W.; Yang, J.H.; Xu, P. Hf isotopic compositions of the standard zircons and baddeleyites used in U-Pb geochronology. *Chem. Geol.* **2006**, *234*, 105–126. [CrossRef]
38. Griffin, W.L.; Pearson, N.J.; Belousova, E.; Jackson, S.E.; Van Achterbergh, E.; O'Reilly, S.Y.; Shee, S.R. The Hf isotope composition of cratonic mantle: LAM-MC-ICPMS analysis of zircon megacrysts in kimberlites. *Geochim. Acta* **2000**, *64*, 133–147. [CrossRef]
39. Nowell, G.M.; Kempton, P.D.; Noble, S.R.; Fitton, J.G.; Saunders, A.D.; Mahoney, J.J.; Taylor, R.N. High precision Hf isotopemeasurements ofMORB and OIB by thermal ionization mass spectrometry: Insights into the depleted mantle. *Chem. Geol.* **1998**, *149*, 211–233. [CrossRef]
40. Belousova, E.A.; Griffin, W.L.; O'Reilly, S.Y. Igneous zircon: Trace element composition as an indicator of source rock type. *Contrib. Mineral. Petrol.* **2002**, *143*, 602–622. [CrossRef]
41. Hoskin, P.W.O.; Schaltegger, U. The composition of zircon and igneous and metamorphic petrogenesis. *Rev. Mineral. Geochem.* **2003**, *53*, 27–62. [CrossRef]
42. Peccerillo, A.; Taylor, S.R. Geochemistry of eocene calc–alkaline volcanic rocks from the Kastamonu area, Northern Turkey. *Contrib. Mineral. Petrol.* **1976**, *58*, 63–81. [CrossRef]
43. Maniar, P.D.; Piccoli, P.M. Tectonic discrimination of granitoids. *Geol. Soc. Am. Bull.* **1989**, *101*, 635–643. [CrossRef]
44. Sun, S.S.; McDonough, W.F. Chemical and isotopic systematics of oceanic basalts: Implications for mantle composition and processes. In *Magmatism in theOcean Basins*; Saunders, A.D., Norry, M.J., Eds.; Geological Society London Special Publications: London, UK, 1989; Volume 42, pp. 313–345.
45. Weaver, B.L. The origin of ocean island basalt end member compositions: Trace element and isotopic constraints. *Earth Planet. Sci. Lett.* **1991**, *101*, 381–397. [CrossRef]
46. Rapp, R.P.; Watson, E.B. Dehydration melting of metabasalt at 8–32 kbar: Implications for continental growthand crust–mantlerecycling. *J. Petrol.* **1995**, *36*, 891–931. [CrossRef]
47. Wu, F.Y.; Li, X.H.; Zheng, Y.F.; Gao, S. Lu-Hf isotopic systematics and their applications in petrology. *Acta Petrol. Sin.* **2007**, *23*, 185–220. (In Chinese with English abstract)
48. Li, S.D.; Zhang, X.B.; Gao, L.L. Ore Genesis at the Jinchang Gold–Copper Deposit in Heilongjiang Province, Northeastern China: Evidence from Geology, Fluid Inclusions, and H–O–S Isotopes. *Minerals* **2019**, *9*, 99. [CrossRef]
49. Saunders, A.D.; Norry, M.J.; Tarney, J. Origin of MORB and chemically-depleted mantle reservoirs: Trace element constraints. *J. Petrol. Spec. Vol.* **1988**, *1*, 415–445. [CrossRef]
50. Mao, J.W.; Zhang, Z.C.; Zhang, Z.H.; Du, A.D. Re–Os isotopic dating of molybdenites in the Xiaoliugou W (Mo) deposit in the northern Qilian mountains and its geologicalsignificance. *Geochim. Cosmochim. Acta* **1999**, *63*, 1815–1818.
51. Shirey, S.B.; Walker, R.J. Carius tube digestion for low-blank rhenium-osmium analysis. *Anal. Chem.* **1995**, *67*, 2136–2141. [CrossRef]
52. Palmer, M.R.; Turekian, K.K. $^{187}Os/^{186}Os$ in marine manganese nodules and the constraints on the crustal geochemistry of rhenium and osmium. *Nature* **1986**, *319*, 216–220. [CrossRef]
53. Zhang, H.F.; Gao, S. *Geochemistry*; Geology Press: Beijing, China, 2012; pp. 232–238. (In Chinese)
54. Yang, H.; Ge, W.C.; Zhao, G.C.; Dong, Y.; Xu, W.L.; Ji, Z.; Yu, J.J. Late Triassic intrusive complex in the Jidong region, Jiamusi–Khanka Block, NE China: Geochemistry, zircon U–Pb ages, Lu–Hf isotopes, and implications for magma mingling and mixing. *Lithos* **2015**, *224–225*, 143–159. [CrossRef]
55. Pearce, J.A.; Harris, N.B.W.; Tindle, A.G. Trace element discrimination diagrams for the tectonic interpretation of granitic rocks. *J. Petrol.* **1984**, *25*, 956–983. [CrossRef]
56. Harris, N.B.W.; Pearce, J.A.; Tindle, A.G. Geochemical characteristics of collision-zone magmatism. *Geol. Soc. Lond. Spec. Publ.* **1986**, *19*, 67–81. [CrossRef]
57. Zhang, Z.C.; Mao, J.W.; Wang, Y.B.; Pirajno, F.; Liu, J.L.; Zhao, Z.D. Geochemistryand geochronology of the volcanic rocks associated with the Dong'an adularia–sericite epithermal gold deposit, Lesser Hinggan Range, Heilongjiang province, NE China: Constraints on the metallogenesis. *Ore Geol. Rev.* **2010**, *37*, 158–174. [CrossRef]
58. Zhang, G.B.; Yang, Y.C.; Wang, J.; Wang, K.Y.; Ye, S.Q. Geology, geochemistry, and genesis of the hot-spring-type Sipingshan gold deposit, eastern Heilongjiang province, Northeast China. *Int. Geol. Rev.* **2013**, *55*, 482–495. [CrossRef]
59. Shu, Q.H.; Chang, Z.; Lai, Y.; Zhou, Y.; Sun, Y.; Yan, C. Regional metallogeny of Mo-bearing deposits in northeastern China, with new Re-Os dates of porphyry Mo deposits in the northern Xilamulun district. *Econ. Geol.* **2016**, *111*, 1783–1798. [CrossRef]
60. Kiminami, K.; Imaoka, T. Spatiotemporal variations of Jurassic-Cretaceous magmatism in eastern Asia (Tan-Lu fault to SW Japan): Evidence for flat-slab subduction and slab rollback. *Terra Nova* **2013**, *25*, 414–422. [CrossRef]
61. Sun, M.D.; Chen, H.L.; Zhang, F.Q.; Wilde, S.A.; Dong, C.W.; Yang, S.F. A 100 Ma bimodal composite dyke complex in the Jiamusi block, northeastern China: An indication for lithospheric extension driven by Paleo-Pacifc roll-back. *Lithos* **2013**, *162–163*, 317–330. [CrossRef]
62. Lallemand, S.; Heuret, A.; Boutelier, D. On the relationships between slab dip, back-arc stress, upper plate absolute motion, and crustal nature in subduction zones. *Geochem. Geophys. Geosyst.* **2005**, *6*, 259. [CrossRef]
63. Maruyama, S.; Okamoto, K. Water transportation from the subducting slab into the mantle transition zone. *Gondwana Res.* **2007**, *11*, 148–165. [CrossRef]

64. Yuan, C.; Sun, M.; Xiao, W.J.; Wilde, S.; Li, X.H.; Liu, X.H.; Long, X.P.; Xia, X.P.; Ye, K.; Li, J.L. Garnet-bearing tonalitic porphyry from East Kunlun, Northeast Tibetan Plateau: Implications for adakite and magmas from the MASH Zone. *Int. J. Earth Sci.* **2009**, *98*, 1489–1510. [CrossRef]
65. Hoffer, G.; Eissen, J.P.; Beate., B. Geochemical and petrological constraints on rear-arc magma genesis processes in Ecuador: The Puyo cones and Mera lavas volcanic formations. *J. Volcanol. Geotherm. Res.* **2008**, *176*, 107–118. [CrossRef]
66. Chen, L.; Tang, L.M.; Yang, J.C.; Li, X.H.; Wang, W.; Chu, F.Y.; Zhang, J. Petrogenesis and tectonic implication of lavas from the Yap Trench, western Pacific. *Acta Oceanol. Sin.* **2021**, *40*, 147–161. [CrossRef]